

# Charge current and phase diagram of the disordered open longer-range Kitaev chain

Emmanuele G. Cinnirella<sup>(1)</sup>, Andrea Nava<sup>(2)</sup>, and Domenico Giuliano<sup>(1,2)</sup>

<sup>(1)</sup> *Dipartimento di Fisica, Università della Calabria Arcavacata di Rende I-87036, Cosenza, Italy and I.N.F.N., Gruppo collegato di Cosenza Arcavacata di Rende I-87036, Cosenza, Italy*

<sup>(2)</sup> *Institut für Theoretische Physik, Heinrich-Heine-Universität, 40225 Düsseldorf, Germany*

(Dated: August 28, 2025)

We compute the disorder averaged dc conductance in the non-equilibrium steady state that sets in between a longer-range Kitaev chain and a metallic lead connected to an external reservoir, as a function of the system parameters and of the disorder strength. From our results, we map out the phase diagram of the disordered chain for different types of disorder and discuss the corresponding effects of the interplay between topology and disorder in the system. To do so, we set up a combined analytical and numerical approach, which is potentially amenable of straightforward generalizations to other disordered topological systems.

## I. INTRODUCTION

Recently, one-dimensional (1D) electronic topological systems have become the subject of an intensive and systematic study, primarily due to their remarkable property of developing (topological) phases characterized by emerging, low-lying, charge-neutral modes, localized at the endpoint(s) of the system [1, 2]. Indeed, the peculiar properties of the localized modes, in particular their robustness against fluctuations in the system operating parameters (including the temperature), disorder, and so on, make them particularly suitable to engineer robust qubits and fault tolerant quantum computing protocols. The emergence of topological phases can be realized in a wide class of solid-state systems [3–7], and has also recently been experimentally seen in optical simulations of topological systems [8, 9].

An effective way to probe topological phases for given system parameters is to compute a topological invariant quantity, such as the Zak phase (the “winding number”)  $\omega$  [10].  $\omega$  is computed in models with periodic boundary conditions: it takes either 0, or nonzero, integer values, and its specific value counts how many independent localized modes emerge at each endpoint of the system with open boundary conditions [11, 12]. Therefore, when  $\omega = 0$  the system lies within a topologically trivial phases, while topological non-trivial phases are signaled by a nonzero value of the topological invariant. Electronic models with short range electron hopping and/or interactions, typically host at most one single localized mode at endpoints of the system, which implies  $|\omega| = 0, 1$ , while models with longer (that is, beyond nearest neighbor) hopping and/or interactions may develop phases with  $|\omega| > 1$ . Such “higher- $\omega$ ” phases are expected to emerge in solid-state systems, both normal [13–16], and superconducting [17–20], as well as in optical systems [8, 9]. Thus, it is important to investigate their properties in pertinently constructed “minimal” prototypical models.

To formally describe realistic topological systems one has to account for the unavoidable effect of disorder. In this respect, the interplay of disorder and topology has several, nontrivial consequences on the phase diagram

of a disordered topological model, with features depending on the model Hamiltonian of the topological system in the “clean” limit, as well as on the specific kind of disorder one considers, together with the related symmetries underneath the disorder potential. For instance, in topological systems with only short range electron hopping strengths and interactions (including pairing interaction in superconducting models), a small amount of Anderson-like disorder may work to enforce the stability of the topological phase, which may “reenter” into regions of values of the Hamiltonian parameters that would be topologically trivial in the clean limit [21–26]. Also, the effects of adding disorder to the model Hamiltonian strongly depend on whether the disorder preserves, or not, some specific symmetries of the system Hamiltonian [27, 28]. Given their richer phase diagram, compared to short range models, it is therefore quite interesting to address the effects of the interplay between disorder and topological phases in systems with more than one topological phase in their phase diagram.

In this paper, we study the phase diagram of the longer range 1D Kitaev Hamiltonian (2LRK): a model of spinless electrons with both first- and second-neighbor single electron hopping terms and first- and second-neighbor pairing terms [17], in the presence of three different kinds of disorder potentials. Specifically, we consider the case of Anderson disorder, of the Aubry-André-Harper model [29, 30], and of a disorder affecting the hopping and the pairing strengths in the model Hamiltonian. In all three cases we have to define a pertinent generalization of  $\omega$ , in order to properly reconstruct the corresponding topological phases in the phase diagram. To do so, we employ an adapted version of the approach used in [23, 26, 28]. Specifically, we focus onto an open 2LRK, connected by one of its sites to a metallic lead. On its own, the lead is connected to an external thermal bath, whose interplay with the system dynamics drives its time evolution toward a pertinent non-equilibrium steady state (NESS), in which a potential bias between the lead and the 2LRK induces a current flow across the interface between the two of them. Estimating, for each single realization of the disorder, the corresponding dc conductance,  $G_{\text{int},n}$ , for each site of the chain and summing over all the sites,

we obtain a quantity given by a prefactor depending only on the total Hamiltonian parameters in the clean limit, times  $\omega$  (which is always quantized), computed for that realization of the disorder. Eventually, by averaging over several realizations of disorder, we construct the corresponding extension of  $\omega$ , from which we infer the phase diagram of the disordered system.

Following the method of Refs.[23, 26, 28], we describe the time evolution of the open system toward the NESS by means of Linblad Master equation (LME) approach [31], which has already been successfully applied to study the onset of dynamical topological phase transitions [32–37], as well as the NESS that sets in the system as a consequence of the coupling to the external reservoir [38–43]. Within LME approach, we recover the time evolution equations for the two-fermion correlation matrix elements, in terms of which we express the dc conductance at each site. In the  $t \rightarrow \infty$  limit, we obtain the correlation matrix elements and, therefore, the dc conductances  $G_{\text{int},n}$  in the NESS. Remarkably, while analytically solving the LME to recover the correlation matrix at any  $t$  is practically impossible, by pertinently adapting the formalism developed in Ref.[44], we are able to provide an analytical expression for  $G_{\text{int}}$  in the weak coupling limit in both the coupling between the chain and the lead and between the lead and the reservoir, at any given realization of the disorder. Eventually, we numerically average our results for  $G_{\text{int}}$  (and, therefore, for  $\omega$ ) over all the realizations of the disorder. Plotting the corresponding average as a function of the tuning Hamiltonian parameter(s) and of the disorder strength  $W$ , we reconstruct the whole phase diagram of the disordered system.

At a synoptic look at our results, we evidence how different kinds of disorder affect the topological phases in the 2LRK. In particular, while we confirm that the uncorrelated (Anderson) disorder enforces (in the weak disorder limit) the  $|\omega| = 1$  topological phase, we also note that it strongly suppresses phases with  $|\omega| = 2$ . At variance, a correlated disorder, can tend to enforce higher- $|\omega|$  topological phases, eventually generalizing to those phases the reentrant behavior of the  $|\omega| = 1$  phase in the presence of Anderson disorder. Throughout our derivation, we evidence how, given its generality and the complementary use of analytical and numerical methods, our approach has a potential range of applicability much wider than the specific cases we analyze here. Moreover, in view of its potential potential experimental implementation [45], it can likely provide a systematic tool to investigate the intriguing interplay between topology and disorder in solid state electronic systems.

The paper is organized as follows:

- In Section II we present the model Hamiltonian for the isolated 2LRK, together with the various types of disorder that we consider. Then, we provide the formal description of the superconducting chain connected to the lead which, on its own, is connected to the external reservoir. Eventually, we

review the LME approach and its application to the specific system that we consider here.

- In Section III we present and discuss our results for the phase diagram of the open 2LRK derived from the dc conductance in the NESS,  $G_{\text{int}}$ .
- In Section IV we summarize our results and provide some possible further developments of our work.
- In Appendix A we provide the details on the mathematical derivation of the dc conductance through the interfaces between the Kitaev chain and the metallic leads.

## II. SYSTEM MODEL HAMILTONIAN

In this Section we provide the model Hamiltonian for the 2LRK, first in the clean limit, and then in the presence of disorder. Eventually, we add a coupling between the Kitaev chain and the metallic lead connected to the external reservoir. Due to the coupling to the reservoir, the superconducting chain and the lead, taken all together, constitute an open system, which we formally treat within LME approach. Therefore, we devote the last part of this Section to review LME formalism and how to apply it to our specific system. In Appendix A we present the mathematical derivation of the electric current through the NS interfaces between the chain and the lead.

### A. Model Hamiltonian for the longer-range Kitaev chain

Kitaev lattice model for a one-dimensional p-wave superconductor has by now become a prototypical system hosting Majorana real fermionic modes localized at the boundaries of a finite chain [46], also in view of the various possible platform that have been proposed as potential realizations of the model [5, 47–49]. Moreover, the Kitaev model is well-known to provide a fermionic description of the one-dimensional quantum Ising model, with the latter model being mapped onto the former via Jordan-Wigner fermionization procedure (see, for instance, [50] and references therein). Specifically, tuning the chemical potential of the system, it is possible to drive it across a topological phase transition between a topological gapped phase, in which the localized Majorana modes emerge at the system boundaries, and a trivial gapped phase, in which no modes are present within the gap. Generalizations of the Kitaev Hamiltonian characterized by both normal single electron hopping, as well as pairing, ranging beyond nearest-neighboring sites only, have been discussed in the recent literature [17, 18, 20, 51–54], also in order to make the model Hamiltonian for the system better fit what one should expect from realistic systems [55, 56]. In fact, allowing

for longer-range fermion hopping/pairing allows for the emergence of novel phases in the phase diagram of the Kitaev chains, such as multi-Majorana phases with several real fermionic zero-modes at the edges of the chain, or phases in which long-range correlations pair the edge Majorana modes in massive Dirac boundary modes, et cetera.

In this paper we focus onto the 2LRK, with fermion hopping and pairing taking place between nearest neighboring and next-to-nearest neighboring sites. Following Ref.[17] we write the model Hamiltonian  $H_{2K}$  over an  $L$ -site open chain as

$$H_{2K} = 2g \sum_{n=1}^L \chi_n^\dagger \chi_n - \lambda_1 \sum_{n=1}^{L-1} \{\chi_n^\dagger \chi_{n+1} + \chi_n^\dagger \chi_{n+1}^\dagger + \text{h.c.}\} - \lambda_2 \sum_{n=1}^{L-2} \{\chi_n^\dagger \chi_{n+2} + \chi_n^\dagger \chi_{n+2}^\dagger + \text{h.c.}\} . \quad (1)$$

In Eq.(1),  $\chi_n$  and  $\chi_n^\dagger$  are the single-fermion annihilation and creation operators at site- $n$ , satisfying the anticommutation algebra  $\{\chi_n, \chi_{n'}^\dagger\} = \delta_{n,n'}$ ,  $2g$  is the uniform chemical potential of the model and, for the sake of simplicity, following [17], we have assumed that the nearest-neighbor single electron hopping and the corresponding pairing strengths are equal to each other and both equal to  $\lambda_1$ , while the next-to-nearest single electron hopping and pairing strengths are both equal to  $\lambda_2$ . Finally, h.c. stands for Hermitian conjugate and the sums ranges over lattice sites consistently with the range of the corresponding terms and with the open boundary conditions on the chain. To diagonalize  $H_{2K}$ , we rewrite it in the Nambu spinor basis as

$$H_{2K} = \sum_{q>0} [c_q^\dagger, c_{-q}] [\vec{\sigma} \cdot \vec{\mathcal{H}}(q)] \begin{bmatrix} c_q \\ c_{-q}^\dagger \end{bmatrix} , \quad (2)$$

with  $\vec{\sigma}$  being the triple of the Pauli matrices and

$$\vec{\mathcal{H}}(q) = 2 \begin{bmatrix} 0 & \lambda_1 \sin(q) + \lambda_2 \sin(2q) \\ \lambda_1 \sin(q) + \lambda_2 \sin(2q) & g - \lambda_1 \cos(q) - \lambda_2 \cos(2q) \end{bmatrix} . \quad (3)$$

The model Hamiltonian in Eq.(1) was originally derived in Ref.[17] by applying the Jordan-Wigner fermionization procedure to the three spin extension of the transverse field Quantum Ising model. Taken as just a fermionic model Hamiltonian for a topological superconductor,  $H_{2K}$  possesses particle-hole, time-reversal and chiral symmetries: it belongs to the BDI class of topological insulators and the topological phases can be characterized in terms of an integer-valued topological invariant  $\omega$ . The single-particle energy spectrum of  $H_{2K}$  is, accordingly, particle-hole symmetric: at any  $q$  there is a pair of associated energy eigenvalues of opposite sign,  $\pm\epsilon_q$ , given by

$$\epsilon_q = 2\sqrt{g^2 + \lambda_1^2 + \lambda_2^2 + 2\lambda_1(\lambda_2 - g)\cos(q) - 2g\lambda_2\cos(2q)} . \quad (4)$$

Apparently, Eq.(4) evidences a fully gapped spectrum, with minimum energy gap  $\Delta_{2K}$  depending on the system parameters (for instance, assuming that  $g, \lambda_1$  and  $\lambda_2$  are all  $> 0$ , for small  $g$  we obtain  $\Delta_{2K} = 2|g - \lambda_1 - \lambda_2|$ ). With periodic boundary conditions, the eigenmodes corresponding to the two solutions in Eq.(4) are given by

$$\eta_{2K,q,\pm} = \sum_{n=1}^L \{[u_{q,n,\pm}]^* \chi_n + [v_{q,n,\pm}]^* \chi_n^\dagger\} , \quad (5)$$

with (in Nambu notation)

$$\begin{bmatrix} u_{q,n,+} \\ v_{q,n,+} \end{bmatrix} = a_+ \begin{bmatrix} \cos\left(\frac{\xi_q}{2}\right) \\ i \sin\left(\frac{\xi_q}{2}\right) \end{bmatrix} e^{iqn} , \quad \begin{bmatrix} u_{q,n,-} \\ v_{q,n,-} \end{bmatrix} = a_- \begin{bmatrix} i \sin\left(\frac{\xi_q}{2}\right) \\ \cos\left(\frac{\xi_q}{2}\right) \end{bmatrix} e^{iqn} , \quad (6)$$

and  $\cos(\xi_q) = (g - \lambda_1 \cos(q) - \lambda_2 \cos(2q))/\epsilon_q$ ,  $\sin(\xi_q) = (\lambda_1 \sin(q) + \lambda_2 \sin(2q))/\epsilon_q$ ,  $a_\pm$  being normalization constants. Over the open chain, subgap localized real fermionic modes may appear at the boundaries of the chain, depending on the specific values of the system parameters. While, strictly speaking, no boundary modes emerge in the (closed) chain with periodic boundary conditions, to count the number of localized real fermionic modes that would be present at each endpoint of the chain with open boundary condition, in the case of a closed longer-range Kitaev Hamiltonian and in the absence of disorder one may compute the Zak phase  $\omega$  [10], given by

$$\omega = \frac{i}{\pi} \int_{\text{BZ}} dq \langle u_q | \partial_q | u_q \rangle , \quad (7)$$

with  $\int_{\text{BZ}} dq$  denoting the integral over the full Brillouin zone (that is,  $\int_0^{2\pi} dq$ ), and  $|u_q\rangle$  being the eigenket corresponding to the energy eigenvalue  $-\epsilon_q$ . In our specific model, we can obtain  $\omega = 0$  (that corresponds to the topologically trivial phase) or  $\omega = 1, 2$  (respectively corresponding to the topological phase with one and two Majorana mode(s) at each edge). Combining the whole set of values of  $\omega$  recovered for different values of the system parameters, one obtains a phase diagram such as the one we draw in Fig.1 by repeating the derivation of Ref.[19], that is, by setting  $g = 1$  and by varying both  $\lambda_1$  and  $\lambda_2$ . Just as in [19], we draw the different phases in color, which allows us to identify at a glance the various phase transition lines, separating regions drawn in different colors. Particularly interesting is the possibility to pertinently act on the parameters so to realize direct phase transitions between phases characterized by any pairs of values of  $\omega$  between 0,1 and 2. As we evidence in the following, the disorder can strongly modify the topology of the phase diagram from what we draw in Fig.1.

Analytically recovering solutions for the Nambu spinors corresponding to the Hamiltonian eigenmodes

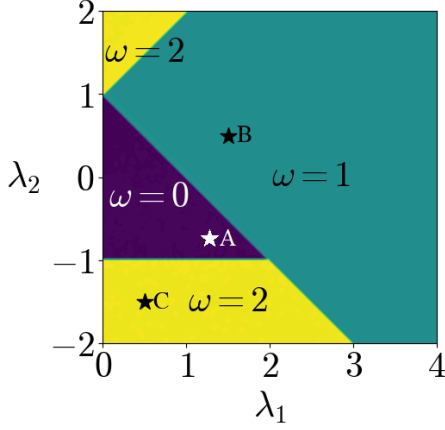


FIG. 1. Phase diagram of the longer-range Kitaev chain with  $g = 1$  in the  $\lambda_1 - \lambda_2$  plane [19]. The various phases are evidenced by different colors: purple for the trivial phase ( $\omega = 0$ ), green for the topological phase with  $\omega = 1$ , yellow for the topological phase with  $\omega = 2$ . In the following, we focus on the points marked with the  $\star$  to provide a first discussion of the effects of adding disorder to the clean system.

over the chain with open boundary conditions requires much more care than in the periodic case (see, for instance, Ref.[57] for a similar analysis performed in the case of the Jordan-Wigner fermionic representation of the quantum spin-1/2 XY spin chain). Alternatively, one may resort to a fully numerical approach, within which one numerically diagonalizes  $H_{2K}$  written in real space, as we do when explicitly computing the current entering a specific site.

We now modify the clean Hamiltonian of Eq.(1) by adding the disorder on top of the clean system.

### B. Disordered longer-range Kitaev chain

Disorder is introduced in many body systems by randomizing one, or more than one, parameters of the system Hamiltonian. Accordingly, physically observable quantities are first computed at a given realization of the disorder and the final results are eventually averaged over all the realizations of the disorder. In topological systems, the interplay between (a moderate amount of) disorder and topology may enforce the topological phase, as compared to the clean limit, while a large value of disorder eventually leads to the disappearance of the topological phase(s) [19, 23–26, 58, 59]. In some cases, some specific generalizations of  $\omega$  can be defined even in the presence of disorder as it is the case, for instance, of the “disorder averaged winding number” (DAWN), which can be unambiguously introduced only in the case in which the disordered Hamiltonian anticommutes with a pertinently defined chiral symmetry operator at any realization of the disorder [27, 60]. In general, however, it is not clear how to detect the topology in the pres-

ence of disorder. (For instance, an alternative means to probe the combined effects of topology and disorder on the system is discussed in [28]).

The phase diagram of the 2LRK with quenched Anderson disorder has been originally studied in Ref.[19] by means of the transfer matrix method and by eventually employing the “entanglement degeneracy criterion” to validate the phase diagram of the disordered system. Here, we generalize the model of [19] to several different types of disorder, as outlined below. Importantly, while the transfer matrix method applies well to the case of Anderson disorder, it is, in general, practically inapplicable to generalizations, such as the ones we consider here, including the case of the open chain connected to external reservoirs. This motivates us to resort to a different mean to characterize the phase diagram of the system by looking at the interface current pattern of the chain connected to the reservoir through a metallic lead, as we discuss in the following of the paper.

Formally, the generic disordered 2LRK model is described by the Hamiltonian

$$H_{2K,d} = 2 \sum_{n=1}^L g_n \chi_n^\dagger \chi_n - \sum_{n=1}^{L-1} \lambda_{1,n} \{ \chi_n^\dagger \chi_{n+1} + \chi_n^\dagger \chi_{n+1}^\dagger + \text{h.c.} \} - \sum_{n=1}^{L-2} \lambda_{2,n} \{ \chi_n^\dagger \chi_{n+2} + \chi_n^\dagger \chi_{n+2}^\dagger + \text{h.c.} \} , \quad (8)$$

with  $\{g_n\}, \{\lambda_{1,n}\}, \{\lambda_{2,n}\}$  being randomly distributed variables. Specifically, in the following we consider three different types of disorder, that is:

**Type 1:** To validate our approach, we study the same system considered in [19], that is, we introduce Anderson disorder by taking  $\{\lambda_{1,n}\}$  and  $\{\lambda_{2,n}\}$  to be uniform and not disordered, while we set  $g_n = \bar{g} + \epsilon_n$  with  $\bar{g} = 1$  and the fluctuating random contributions  $\{\epsilon_n\}$  to be distributed following a uniform distribution such that  $\epsilon_n \in [-\frac{\sqrt{3}W}{2}, \frac{\sqrt{3}W}{2}]$ , with  $W$  being the strength of the disorder.

**Type 2:** As a first example of correlated disorder in the chemical potential, we consider an Aubry-André-Harper model [29, 30], with  $g_n$  realized by the quasi-periodic function  $g_n = \bar{g} + \frac{W}{2} \cos(2\pi\beta n + \phi)$  with  $\bar{g} = 1$ ,  $W$  being the disorder strength,  $\beta = \frac{\sqrt{5}-1}{2}$  being the disorder period (incommensurate to the lattice period), and  $\phi \in [0, 2\pi)$  being a random phase.

**Type 3:** Finally, we consider a correlated bond disorder (mimicking for example a shrinking or expansion of a link connecting two nearest neighboring sites and/or the presence of random magnetic fluxes [27, 61]). The disorder affects all the hoppings and the pairing strengths connected to the link. For each link connecting sites  $n$  and  $n+1$  the disorder acts on  $\lambda_{1,n}$ ,  $\lambda_{2,n}$  and  $\lambda_{2,n-1}$ . In particular, we associate a probability  $p_1$  to the case that the link is not affected by disorder, a probability  $p_2$  to



the case that the hopping and pairing strengths associated to the link increase, and a probability  $p_3 = 1 - p_1 - p_2$  that the hopping and pairing strengths decrease (in the following we consider  $p_1 = p_2 = p_3 = 1/3$ ). When the strengths increases(decreases), we set  $\lambda_{1,n} = \lambda_1 \pm W$ ,  $\lambda_{2,n} = \lambda_2 \pm W$ , and  $\lambda_{2,n-1} = \lambda_1 \pm W$ , with  $W$  being the disorder strength and  $\lambda_1$  and  $\lambda_2$  being the values of the next- and second next-neighbor hopping and pairing strengths respectively, in the clean limit.

To spell out the effects of the various types of disorder on the energy levels of the 2LRK, we now proceed by generating, for each kind of disorder, a given number of configurations of the disorder, and by computing the energy spectrum for each disorder configuration. Eventually, we average the spectrum over all the disorder configurations. On going through that procedure within a given window of the disorder strength  $W$ , we eventually draw plots of the low-lying energy levels as a function of  $W$ . In Figs.2,3,4 we show the corresponding results for the first three energy eigenvalues in the case, respectively, of Anderson disorder, of the Aubry-André-Harper model, and of the correlated bond disorder. In any one of the three cases we have drawn the plots for the chain with  $g = 1$ ,  $L = 100$  sites, and  $\lambda_1 = 1.25, \lambda_2 = -0.75$  (trivial phase - panel **a**)),  $\lambda_1 = 1.5, \lambda_2 = 0.5$  (topological phase with  $\omega = 1$  - panel **b**)),  $\lambda_1 = 0.5, \lambda_2 = -1.5$  (topological phase with  $\omega = 2$  - panel **c**)). The three points are marked as *A*, *B* and *C* in Fig.1, respectively. Since, as an effect of the energy spreading due to the disorder, we have a distribution of energy eigenvalues for each level, in all the figures we followed the drawing code used in Ref.[26] and depict with a solid line the average energy of each level (blue for the lowest energy level, orange for the next to lowest energy level, and green for the next to the next to lowest energy level), over 50 disorder realizations, with the shaded area around each solid line representing the energy eigenvalue dispersion. In the trivial phase (panels **a**)) there are no real fermionic states at zero energy. As  $W = 0$  all three the low-lying states are located at energies larger than the superconducting gap. Remarkably, on increasing  $W$ , the lowest-energy state, at some point, is pulled down to zero energy, thus featuring what one would expect in the  $\omega = 1$  topological phase. Such a tendency to generate a “reentrant topological phase” is known to take place, for instance, in the short-range Kitaev model in the presence of Anderson disorder [24, 25, 59]. Here, we evidence how the feature is general with respect to both the range of electron hopping and/or pairing in the Kitaev model and the specific kind of disorder one is considering. Panels **b**) and **c**), drawn for the system within a topological phase, show a similar trend, for a limited amount of disorder, to generate a reentrant topological phase.

To further evidence the revival/enforcement of the topological phases at a limited  $W$ , in the inset of all panels we show the full spectrum of the chain, averaged over 50 disorder realizations, taken at the value of  $W$  corresponding to the vertical, dashed line in the main plots.

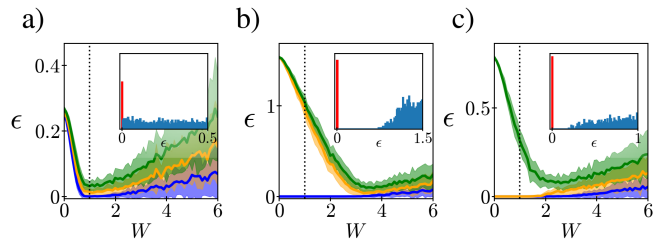


FIG. 2. Plot of the lowest three disorder averaged energy eigenvalues as a function of the Anderson disorder strength  $W$  for the longer-range Kitaev chain with  $g = 1$ ,  $L = 100$  sites, and  $\lambda_1 = 1.25, \lambda_2 = -0.75$  (trivial phase - panel **a**)),  $\lambda_1 = 1.5, \lambda_2 = 0.5$  (topological phase with  $\omega = 1$  - panel **b**)),  $\lambda_1 = 0.5, \lambda_2 = -1.5$  (topological phase with  $\omega = 2$  - panel **c**)) and 50 disorder realizations. The solid lines represent the average energy of the low-lying level (blue), of the next to low lying level (orange), and of the next to the next to the low lying level (green). The shaded area around the solid line measures the standard deviation of the energy eigenvalues around the average value.

Inset (in all three cases): averaged level distribution computed at the value of  $W$  corresponding to the dashed, vertical line.

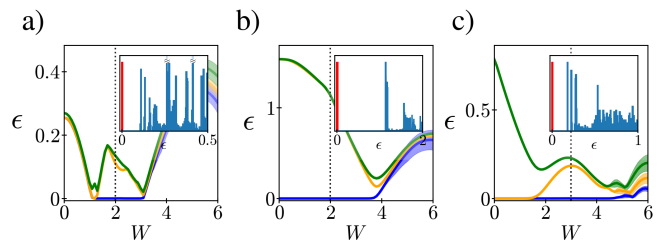


FIG. 3. Plot of the lowest three disorder averaged energy eigenvalues as a function of the AAH disorder strength  $W$  for the longer-range Kitaev chain with  $g = 1$ ,  $L = 100$  sites, and  $\lambda_1 = 1.25, \lambda_2 = -0.75$  (trivial phase - panel **a**)),  $\lambda_1 = 1.5, \lambda_2 = 0.5$  (topological phase with  $\omega = 1$  - panel **b**)),  $\lambda_1 = 0.5, \lambda_2 = -1.5$  (topological phase with  $\omega = 2$  - panel **c**)) and 50 disorder realizations. The solid lines represent the average energy of the low-lying level (blue), of the next to low lying level (orange), and of the next to the next to the low lying level (green). The shaded area around the solid line measures the standard deviation of the energy eigenvalues around the average value.

Inset (in all three cases): averaged level distribution computed at the value of  $W$  corresponding to the dashed, vertical line.

In all three cases we clearly identify a sharp peak pinned at zero energy, which corresponds to the localized real fermionic zero mode that marks the topological phase.

Comparing with each other the plots drawn for the same values of the system parameters, but for different kinds of disorder, we note that the energy broadening for the Anderson and for the correlated bond disorder is of the same order of magnitude, at any values of the parameters. Instead, in the AAH case we see almost no level broadening, which is consistent with fact that in this case it is just the discommensurability effects that mimic a disorder-induced randomness. Finally, we note

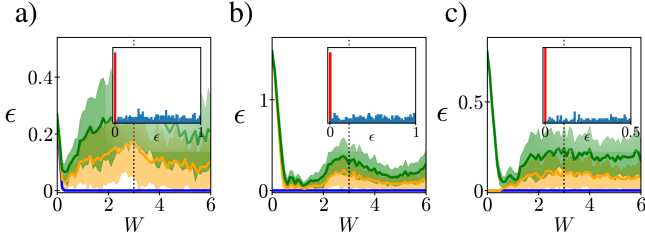


FIG. 4. Plot of the lowest three disorder averaged energy eigenvalues as a function of the correlated bond disorder strength  $W$  for the longer-range Kitaev chain with  $g = 1$ ,  $L = 100$  sites, and  $\lambda_1 = 1.25, \lambda_2 = -0.75$  (trivial phase - panel **a**)),  $\lambda_1 = 1.5, \lambda_2 = 0.5$  (topological phase with  $\omega = 1$  - panel **b**)),  $\lambda_1 = 0.5, \lambda_2 = -1.5$  (topological phase with  $\omega = 2$  - panel **c**)) and 50 disorder realizations. The solid lines represent the average energy of the low-lying level (blue), of the next to low lying level (orange), and of the next to the next to the low lying level (green). The shaded area around the solid line measures the standard deviation of the energy eigenvalues around the average value.

Inset (in all three cases): averaged level distribution computed at the value of  $W$  corresponding to the dashed, vertical line.

that, in all three the cases, at different values of  $W$  and over different energy scales, all the levels are fully gapped at a large enough disorder strength, which is a signal of the fact that a strong amount of disorder fully washes out nontrivial topological phases.

In the following, we extend our formalism to describe the dynamics of the open chain, connected via a metallic lead to the external reservoir, by means of the LME approach.

### C. Formal description of the chain connected to the external reservoirs via a metallic lead: review of Lindblad Master Equation approach

To induce electric current in the 2LRK, we connect one of its sites to an external metallic lead, so that, in its full generality, the Hamiltonian of the resulting system reads  $H = H_L + H_{2K} + H_T$ , with:

$$\begin{aligned} H_L &= -t \sum_{i=1}^{\mathcal{N}-1} \{\alpha_i^\dagger \alpha_{i+1} + \text{h.c.}\} \\ H_T &= -\gamma \{\alpha_{\mathcal{N}}^\dagger \chi_n + \text{h.c.}\} \end{aligned} \quad (9)$$

In Eq.(9) we formally describe the metallic lead as a one-dimensional, spinless, noninteracting lattice electron model at zero chemical potential and with hopping strength  $t$ , over an  $\mathcal{N}$ -site lattice [62–64]. Accordingly, we denote with  $\alpha_i, \alpha_i^\dagger$  the single-electron annihilation and creation operators at site- $i$ , so that we get  $\{\alpha_i, \alpha_{i'}^\dagger\} = \delta_{i,i'}$ , with all the other anticommutators being equal to 0.  $H_T$  corresponds to the single-electron tunneling operator between the endpoint of the lead and

site- $n$  of the superconducting chain, with corresponding tunneling strength equal to  $\gamma$ . The lead and the superconducting region constitute an hybrid system which, following the approach developed in [44], we now couple to the external reservoir only through the lead. Specifically, we regard the reservoir as a source/sink of particles entering/exiting the lead at a given rate, which we specify in the following. In this respect, the whole NS system works as an open system and, in addition, by keeping at a finite voltage bias the reservoir coupled to the lead, we inject/extract a finite current into the superconducting chain, through the metallic lead (note that, since the key quantity we look at here is the dc conductance between the lead and the Kitaev chain, differently from what is done in [65], we indirectly couple the Lindblad bath to the superconductor via the metallic lead). To describe the dynamics of our whole system, we resort to LME approach [31]. Specifically, we write the Schrödinger equation for the density matrix of the system,  $\rho(t)$ , in the form

$$\frac{d\rho(t)}{dt} = -i[H, \rho(t)] + \mathcal{D}[\{\rho(t)\}] \quad (10)$$

In Eq.(10),  $H$  is the total system Hamiltonian, while  $\mathcal{D}[\{\rho(t)\}]$  is the so-called Lindbladian, which we are going to define next.

As a first step, we separately consider the Hamiltonian for the disconnected N and S regions, that is, we pretend that  $\gamma = 0$ , and diagonalize the two of them separately. Denoting with  $\eta_{L,k}$  the eigenmodes of the lead, we get

$$\eta_{L,k} = \sum_{j=1}^{\mathcal{N}} \sqrt{\frac{2}{\mathcal{N}+1}} \sin(kj) \alpha_j \quad (11)$$

with  $k = \frac{\pi\nu}{\mathcal{N}+1}$ , and  $\nu = 1, \dots, \mathcal{N}$  and the corresponding single-particle energy  $\epsilon_k = -2t \cos(k)$ . Next, we choose the Lindblad jump operators, so to stabilize a NESS in which particles injected/extracted through the leads are distributed according to Fermi distribution function. Following Refs.[23, 26, 28, 63], we construct the jump operators for the lead,  $L_{(k,\text{in/out})}$ , so that

$$\begin{aligned} L_{(L,k,\text{in})} &= \sqrt{f(\epsilon_k, V, T)} \eta_{L,k}^\dagger \\ L_{(L,k,\text{out})} &= \sqrt{[1 - f(\epsilon_k, V, T)]} \eta_{L,k} \end{aligned} \quad (12)$$

with the Fermi distribution for the reservoir  $f(\epsilon_k, V, T) = \{1 + \exp[\frac{\epsilon_k - V}{T}]\}^{-1}$  and  $V$  being the bias of the reservoir connected to the lead. Given Eqs.(12), we define  $\mathcal{D}[\{\rho\}]$  as

$$\mathcal{D}[\{\rho(t)\}] = 2\Gamma \sum_{\lambda} \left( L_{\lambda} \rho(t) L_{\lambda}^\dagger - \frac{1}{2} \{L_{\lambda}^\dagger L_{\lambda}, \rho(t)\} \right) \quad (13)$$

with  $\lambda \in \{(k, \text{in}), (k, \text{out})\}$ . Also, in Eq.(13) we have chosen the coupling  $\Gamma$  between the leads and the reservoirs to be independent of the quantum numbers associated to the eigenmodes, so to avoid unnecessary complications

in the following derivation. Similarly to what we do in Eqs.(11), we introduce the eigenmodes of the open, isolated Kitaev chain,  $\eta_{2K,q}$ , by means of the Bogoliubov-Valatin transformations

$$\begin{aligned}\eta_{2K,q} &= \sum_{n=1}^L \{u_{q,n}\chi_n + v_{q,n}\chi_n^\dagger\} \\ \eta_{2K,q}^\dagger &= \sum_{n=1}^L \{[v_{q,n}]^*\chi_n + [u_{q,n}]^*\chi_n^\dagger\} .\end{aligned}\quad (14)$$

Using Eqs.(11,14), we may rewrite the Hamiltonian  $H$  as

$$H = \sum_{\alpha,\beta} \{ \eta_\alpha^\dagger A_{\alpha,\beta} \eta_\beta + \eta_\alpha^\dagger B_{\alpha,\beta} \eta_\beta^\dagger + \eta_\alpha B_{\beta,\alpha}^* \eta_\beta \} , \quad (15)$$

with  $\alpha, \beta \in \{(L, k), (2K, q)\}$  and the matrices  $A$  and  $B$  defined from the Hamiltonian expressed in terms of the whole set of the  $\eta$ -operators. Importantly, the presence of the superconducting block, corresponding to the longer-range Kitaev chain, yields the anomalous pairing terms at the right hand side of Eq.(15), encoded in the nonzero  $B$  matrix.

Using LME approach reviewed above, in the following we compute the current exchanged between the lead and site- $n$  of the superconducting chain, which we use to map out the phase diagram of the longer-range disordered Kitaev chain. To do so, the key quantity we need is the correlation matrix  $\theta(t)$ , together with its anomalous counterpart,  $\theta^A(t)$ . Their matrix elements are respectively defined as

$$\begin{aligned}\theta_{\alpha,\beta}(t) &= \text{Tr}\{\eta_\alpha^\dagger \eta_\beta \rho(t)\} \\ \theta_{\alpha,\beta}^A(t) &= \text{Tr}\{\eta_\alpha^\dagger \eta_\beta^\dagger \rho(t)\} .\end{aligned}\quad (16)$$

Starting from Eq.(10), we now write the time evolution equations for  $\theta(t)$  and for  $\theta^A(t)$ . In doing so, the crucial point is that the set of equations for the corresponding matrix elements is closed, that is, no time-dependent correlation functions of more than two single-particle operators are involved. As a result, we obtain [26]

$$\begin{aligned}\frac{d\theta(t)}{dt} &= i[A^T, \theta(t)] + 2i(\theta^A(t)B + B^*[\theta^A(t)]^\dagger) \\ &\quad - \frac{1}{2} \{G + R, \theta(t)\} + G , \\ \frac{d\theta^A(t)}{dt} &= i(\theta^A(t)A + A^T\theta^A(t)) - 2i(B^*\theta^T(t) + \theta(t)B^*) \\ &\quad - \frac{1}{2} \{G + R, \theta^A(t)\} + 2iB^* ,\end{aligned}\quad (17)$$

with  $T$  denoting the matrix transpose. We have already defined the matrices  $A$  and  $B$  in Eqs.(15). The  $G$  and  $R$  matrix elements are, instead, defined as

$$\begin{aligned}G_{\alpha,\beta} &= 2 \Gamma \delta_{\alpha,\beta} f_\alpha \\ R_{\alpha,\beta} &= 2 \Gamma \delta_{\alpha,\beta} \{1 - f_\alpha\} ,\end{aligned}\quad (18)$$

with

$$f_\alpha = \begin{cases} f(\epsilon_k, V, T) & \text{if } \alpha = (L, k) \\ 0 & \text{if } \alpha = (2K, q) \end{cases} . \quad (19)$$

In the following, we employ Eqs.(17) to compute the current across the NS interfaces in the non-equilibrium steady state of our system.

### III. DC CONDUCTANCE IN THE NON-EQUILIBRIUM STEADY STATE AND PHASE DIAGRAM OF THE DISORDERED SYSTEM

The dc current at the NS interface between the endpoint of the normal lead and the  $n$ -th site of the longer-range Kitaev chain is given by (see Eq.(A10) for the definition of the corresponding operator)

$$I_{\text{int},n} = -i\gamma \{ \langle \alpha_{\mathcal{N}}^\dagger \chi_n \rangle - \langle \chi_n^\dagger \alpha_{\mathcal{N}} \rangle \} , \quad (20)$$

with  $\langle \dots \rangle$  denoting the expectation value of the operator computed in the system at the NESS. In Appendix A we discuss in detail how to compute the average values of the bilinear of fermionic operators at the right-hand side of Eq.(20) in terms of the correlation matrices at the NESS,  $\theta_{\text{NESS}}$  and  $\theta_{\text{NESS}}^A$ . The key point in using the quantity in Eq.(20) to compute the topological invariant of the system is that, as we prove in Appendix A, the system itself lies within a gapped phase. Within linear response theory in the voltage bias  $V$  between the metallic lead and the superconducting chain, one obtains

$$I_{\text{int}} = \sum_{n=1}^L I_{\text{int},n} = G_{\text{int}} V , \quad (21)$$

with the total dc conductance being given by

$$G_{\text{int}} = \frac{2\gamma^2}{\pi t \Gamma} \left[ 1 + \left( \frac{\Gamma}{2t} \right)^2 \right] \omega . \quad (22)$$

In Eq.(9), the parameters  $t$  and  $\gamma$  respectively correspond to the single-fermion hopping strength between nearest neighboring sites of the metallic leads and between the endpoint of the lead and the site  $n$  of the 2LRK.  $\Gamma$  is introduced in Eq.(13) and corresponds to the coupling strength between the superconducting chain and the Lindblad bath.  $\omega$  is the winding number, basically counting the number of localized, subgap states that set in within the topological phase. As a result, we find that, by fixing the system parameters and measuring  $G_{\text{int}}$  in units of  $G_{\text{int}}^{(0)} = \frac{2\gamma^2}{\pi t \Gamma} \left[ 1 + \left( \frac{\Gamma}{2t} \right)^2 \right]$ , one directly gets

$$\frac{G_{\text{int}}}{G_{\text{int}}^{(0)}} = \omega . \quad (23)$$

Eq.(23) is the key relation behind the derivation of this Section, where we employ the result of the numerical

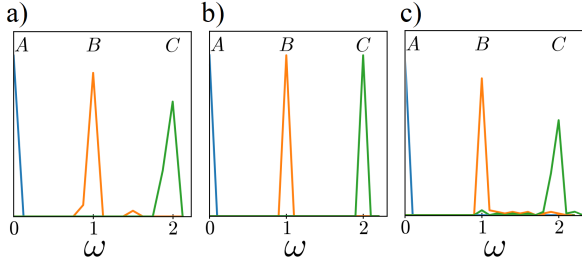


FIG. 5. Histograms of  $\omega$ , extracted from the dc conductance in Eq.(22) between a normal lead connected to a longer-range Kitaev chain and the chain itself, in the presence of different types of disorder (see Sec.IIB). In all panels we set  $\mathcal{N} = L = 50$ ,  $g = 1$ ,  $t = 0.05$ ,  $\gamma = 0.01$ ,  $\Gamma = 0.005$  and  $\lambda_1 = 0.5$ . Points  $A$ ,  $B$  and  $C$  correspond to different values of  $\lambda_2$  and  $W$ . Specifically, we consider the following kinds of disorder: Panel **a**): Anderson disorder (Type 1) for  $\lambda_{2,A} = -0.6$ ,  $W_A = 0.5$ ,  $\lambda_{2,B} = 0.8$ ,  $W_B = 1.5$ , and  $\lambda_{2,C} = -1.6$ ,  $W_C = 2.5$ ; Panel **b**): Aubry-André-Harper correlated disorder (Type 2) for  $\lambda_{2,A} = -0.8$ ,  $W_A = 0.3$ ,  $\lambda_{2,B} = -0.8$ ,  $W_B = 2.0$ , and  $\lambda_{2,C} = -1.8$ ,  $W_C = 2.0$ ; Panel **c**): correlated bond disorder (Type 3) for  $\lambda_{2,A} = -0.8$ ,  $W_A = 0.3$ ,  $\lambda_{2,B} = -0.8$ ,  $W_B = 1.0$  and  $\lambda_{2,C} = -1.8$ ,  $W_C = 4.5$ .

calculation of the dc conductances, in the clean limit as well as in the presence of disorder, to map out the whole phase diagram of our system. Indeed, Eq.(23) is expected to keep valid in the presence of disorder, as long as the energy of the subgap states induced by disorder is greater than the applied bias  $V$ . However, as we will show in the following, also for strong disorder (at least for  $W \approx 3 \times \max(g, \lambda_1, \lambda_2)$ ), the (disorder averaged)  $\omega$  proves to be a robust probe of the topological phase, due to the fact that the non-quantized contribution to the conductance due the “bulk”, over the gap, states (Eq.(A15) of Appendix A), is much smaller than the topological one (Eq.(A16)), proportional to  $\omega$ . Furthermore, in order to probe  $\omega$  for greater values of  $W$  and/or for non-zero temperature,  $T$ , one can extract the zero-bias conductance with higher precision (thus washing out the contribution of the disorder induced subgap state) by increasing the length of the normal lead, and thus having access to lower values of  $V$ , or by implementing a logarithmic-linear discretization scheme for the normal lead density of states [62, 63].

In the following we numerically compute  $\omega$  setting  $\mathcal{N} = L = 50$ ,  $g = 1$ ,  $t = 0.05$ ,  $\gamma = 0.01$  and  $\Gamma = 0.005$ . Although working in the small- $V$  limit, we carefully take  $V$  larger than the finite-size gap of the metallic lead, so to avoid spoiling of our results by finite-size effects. Finally, we fix  $\lambda_1 = 0.5$  and investigate the phase diagram of the disordered 2LRK as a function of the next-to-nearest single electron hopping and pairing strengths  $\lambda_2$  and of the disorder strength  $W$  for the three types of disorder introduced in Sec.IIB.

To check that the quantization of  $\omega$  holds also in presence of disorder, in Fig.5 we plot an histogram of the values

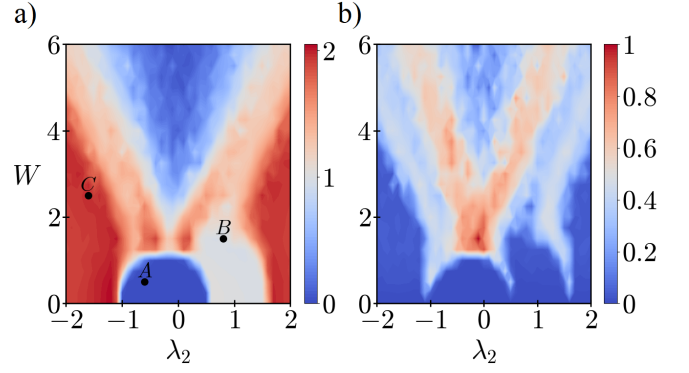


FIG. 6. Phase diagram of the longer-range Kitaev model of length  $L = 50$  and Type 1 disorder in the  $\lambda_2 - W$  plane. The other parameters are the same as in Fig.5. Panel **a**)  $\bar{\omega}$  averaged over 100 disorder realizations. Points  $A$ ,  $B$  and  $C$  are the same as listed in Fig.5a). Panel **b**) standard deviation of  $\bar{\omega}$ .

of  $\omega$ , extracted from the numerical results for  $G_{\text{int}}$  computed for 100 realizations of the disorder and for different combinations of  $(\lambda_2, W)$ .

In Fig.5a) we plot the distribution of values of  $\omega$  for the Anderson disorder, with points  $A$ ,  $B$  and  $C$  corresponding to the following pairs of values of  $(\lambda_2, W)$ :  $A = (-0.6, 0.5)$ ,  $B = (0.8, 1.5)$  and  $C = (-1.6, 2.5)$ . Case  $A$  shows an histogram peaked at  $\omega_A = 0$ , corresponding to a point of the phase diagram in a topologically trivial phase, hosting no topological states; the histogram for case  $B$  is peaked around  $\omega_B = 1$ , a signature of a topologically nontrivial phase hosting a single topological state at each boundary; finally, case  $C$  histogram is peaked around  $\omega_C = 2$ , associated to a topologically nontrivial phase with two topological states at each boundary. A similar result holds in Fig.5b), for the Aubry-André-Harper disorder, where we have chosen  $A = (-0.8, 0.3)$ ,  $B = (-0.8, 2.0)$  and  $C = (-1.8, 2.0)$  and in Fig.5c), Type 3 disorder (correlated bond disorder), with  $A = (-0.8, 0.3)$ ,  $B = (-0.8, 1.0)$  and  $C = (-1.8, 4.5)$ . It is worth to note that, even for high values of  $W$ , the quantization of  $\omega$  is preserved.

In Fig.6 we reconstruct the phase diagram in the  $\lambda_2 - W$  plane for the Type 1 disorder. In panel **a**) we show the mean value of  $\omega$  over 100 disorder realization,  $\bar{\omega}$ , while in panel **b**) the provide corresponding standard deviation. (We also highlight the points  $A$ ,  $B$  and  $C$  shown in Fig.5a)) The phase diagram exhibits bulk areas of uniform color and low values of the standard deviation. In these regions  $\bar{\omega}$  is equal to 0 (no topological states), 1 (one topological state at each boundary) and 2 (two topological states for boundary). These bulk areas are separated by extended regions characterized by intermediate values of  $\bar{\omega}$  and high values of the standard deviation, where the topological phase transitions take place. Along the phase transitions, despite a non quantized value of  $\bar{\omega}$ , for each disorder realization we have a well quantized value of  $\omega$ . The histograms of  $\omega$  in these regions show a bimodal dis-



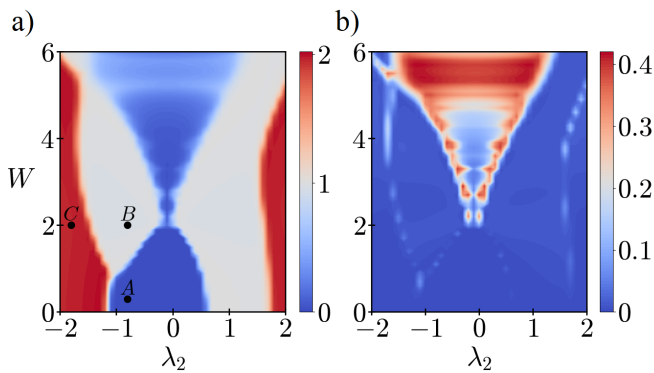


FIG. 7. Phase diagram of the longer-range Kitaev model of length  $L = 50$  and Type 2 disorder in the  $\lambda_2 - W$  plane. The other parameters are the same as in Fig. 5. Panel a)  $\bar{\omega}$  averaged over 100 disorder realizations. Points A, B and C are the same as listed in Fig. 5b). Panel b) standard deviation of  $\bar{\omega}$ .

tribution peaked around integer values of  $\omega$  with different reciprocal altitudes of the peaks, similar to the Griffiths phase observed in many topological models and by means of several topological invariants [25, 26, 28, 48, 66]. Focusing on Fig. 6a) some interesting features emerge. At weak disorder, around  $\lambda_2 = 0$ , the topological trivial phase, blue region, characterized by  $\bar{\omega} = 0$ , fades away and is replaced by the grey and the red regions. This is a signature of a disorder induced reentrant topological phase transition. In favor of phases hosting a single or two topological modes at each boundary [21, 24, 25]. Further increasing disorder strength drives again the system toward a topological trivial phase, washing out the presence of the topological states. It is worth to note that the phase diagram derived in our paper for the Anderson disorder, by computing the interface current, agrees with the one analytically predicted in [19] by transfer matrix and entanglement metrics techniques. However, analytical approaches, like the one in [19] or, as well, the strong disorder renormalization group approach [67–69], typically provide sharp transitions lines, without the possibility of resolving the transition regions that separate different topological phases [23].

In Fig. 7 we show  $\bar{\omega}$  and its standard deviation in the  $\lambda_2 - W$  plane for the Type 2 disorder. The Aubry-André-Harper disorder is a correlated disorder characterized by some interesting properties. First, compared to Anderson disorder, in one-dimensional models it exhibits a localization transition for a finite value of disorder strength [70, 71]. Second, in long range topological models it can lead to the creation of disorder generated topological modes [72]. Both features can be observed in Fig. 7a). Indeed, for  $W < 0.5$  there is barely no effect due to the disorder while we observe the onset of a reentrant topological phase for the phase with  $\omega = 1$  (grey area) only for  $W > 0.5$ . This transition is similar to the one observed for Anderson disorder and is due the fact that a weak localization is known to protect the topological

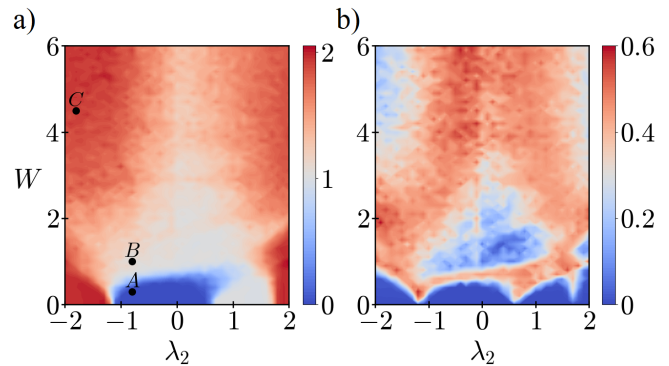


FIG. 8. Phase diagram of the longer-range Kitaev model of length  $L = 50$  and Type 3 disorder in the  $\lambda_2 - W$  plane. The other parameters are the same as in Fig. 5. Panel a)  $\bar{\omega}$  averaged over 100 disorder realizations. Points A, B and C are the same as in Fig. 5c). Panel b) standard deviation of  $\bar{\omega}$ .

states [25]. However, this property does not hold for the topological phase with  $\bar{\omega} = 2$  (red area) that retreats with increasing  $W$ . Starting from  $W \approx 2$  the  $\bar{\omega} = 0$  region begins to expand, as also observed for Type 1 disorder. Eventually, a strong enough disorder is expected to suppress nontrivial topological phases. Compared with the Type 1 disorder, the boundary regions are now much sharper, as highlighted by a small standard deviation in almost the entire phase diagram, see Fig. 7b). However, for  $W > 5$ , we observe a transition from a trivial phase towards a topological non trivial phase, together with a sharp increase of the standard deviation. Contrarily to the reentrant topological phase transition observed for lower values of disorder, we expect that this high disorder region is due the creation of disorder generated topological modes similar to the ones observed in the infinite range Kitaev model [72].

Finally, in Fig. 8 we show  $\bar{\omega}$  and its standard deviation in the  $\lambda_2 - W$  plane for the correlated disorder of Type 3. At weak disorder strength this type of disorder quickly suppresses both the topological trivial phase (blue area) and the  $\bar{\omega} = 2$  topological one, in favor of the topological phase with  $\bar{\omega} = 1$ . However, for strong disorder, compared to the other types of disorder, the trivial phase is not recovered and, on the contrary we have a second reentrant topological transition in favor of the  $\bar{\omega} = 2$  phase, with a drastic reduction of the standard deviation around  $\lambda_2 = \pm 2$ . In conclusion, we have shown that, for non-correlated Anderson disorder (Type 1), a reentrant topological transition is possible in the low disorder region of the phase diagram, while stronger values of the disorder tend to wash out the topological states. On the contrary, correlated disorder (Type 2 and Type 3) can protect, and eventually generate, the topological phases also at high values of the disorder strength.

#### IV. CONCLUSIONS

In this paper we compute the disorder averaged dc conductance between a metallic lead connected to a site of a disordered 2LRK, and the chain itself, in the NESS toward which the system evolves on connecting the lead to an external reservoir. Varying the parameters of the 2LRK Hamiltonian and the disorder strength, we use our results to map out the whole phase diagram of our system, for three different types of disorder. Doing so, we are able to evidence how disorder affects the different topological phases that set in the 2LRK in the clean limit, eventually showing how, while (a weak amount of) Anderson disorder enforces low- $|\omega|$  topological phases, while suppressing phases with higher winding number, the other two types of (correlated) disorder further stabilize the higher- $|\omega|$  phases, as well, or allow for a reentrant topological phase at strong disorder.

Given its generality and its ease of implementation, our approach is amenable of straightforward generalizations to topological systems with a more complex phase diagram than the 2LRK and in more complex geometries [20, 73–76], thus providing a general and quite effective method to unveil the intriguing interplay between disorder and topology in topological superconducting systems.

#### ACKNOWLEDGMENTS

A. N. acknowledges funding by the Deutsche Forschungsgemeinschaft (DFG, German Research Foundation), Projektnummer 277101999 – TRR 183 (project B02), under project No. EG 96/13-1, and under Germany’s Excellence Strategy – Cluster of Excellence Matter and Light for Quantum Computing (ML4Q) EXC 2004/1 – 390534769. E. G. C. acknowledges funding (partially) supported by ICSC Centro Nazionale di Ricerca in High Performance Computing, Big Data and Quantum Computing, funded by European Union NextGenerationEU and thanks the Quantum Matter Institute - Vancouver, for the kind hospitality during the completion of this work. The data underlying the figures in this work can be found at the zenodo site: <https://doi.org/10.5281/zenodo.16947234>

#### Appendix A: Mathematical derivation of the dc conductance through the interfaces between the Kitaev chain and the metallic leads

In this Appendix we derive the formula for the dc conductance between the metallic lead and a site of the 2LRK and discuss its relation with the (disorder averaged)  $\omega$ . To do so, we rely on the formalism of Ref.[44], although pertinently adapted to our problem. To make the presentation of our method the clearest it is possible, in the following we summarize the various formal steps in a sequence of subsections. While, strictly speaking, the

approach we present here applies in the clean limit only, it provides an important guideline to the extension of our method to the disordered system, which we present in the main text.

##### 1. Nambu representation and generalized Lindblad equation for the correlation matrix elements

To ease the following formal steps, we define the  $(2(\mathcal{N} + L) \times 2(\mathcal{N} + L))$  correlation matrix in Nambu basis,  $\Theta(t)$ , as

$$\Theta(t) = \begin{bmatrix} \theta(t) & \theta^A(t) \\ (\theta^A(t))^\dagger & \mathbf{I} - \theta^T(t) \end{bmatrix}, \quad (\text{A1})$$

with  $\mathbf{I}$  being the identity matrix. In terms of  $\Theta(t)$ , we can rewrite Eqs.(17) in a compact form as

$$\frac{d\Theta(t)}{dt} = i[\mathcal{K}, \Theta(t)] - \frac{1}{2} \{ \mathcal{G} + \mathcal{R}, \Theta(t) \} + \mathcal{G}, \quad (\text{A2})$$

with

$$\mathcal{K} = \begin{bmatrix} A^T & -2B^\dagger \\ -2B & -A \end{bmatrix}, \quad (\text{A3})$$

and

$$\mathcal{G} = \begin{bmatrix} G & \mathbf{0} \\ \mathbf{0} & R \end{bmatrix}, \quad \mathcal{R} = \begin{bmatrix} R & \mathbf{0} \\ \mathbf{0} & G \end{bmatrix}. \quad (\text{A4})$$

Eq.(A2) is the key ingredient required to derive the correlation matrix characterizing the non-equilibrium steady state,  $\Theta_{\text{NESS}}$ , which has to be independent of time and, therefore, has to satisfy the equation  $\frac{d\Theta_{\text{NESS}}(t)}{dt} = 0$ . To explicitly solve it for  $\Theta_{\text{NESS}}$ , we write it in a series expansion of the couplings between the superconducting chain and the metallic lead,  $\gamma$ . Specifically, we set

$$\Theta_{\text{NESS}} = \sum_{n=0}^{\infty} \gamma \Theta_{\text{NESS},n}, \quad (\text{A5})$$

and, to rewrite the full condition for the non-equilibrium steady state as a set of recursive equations for the  $\Theta_n$ ’s, we split  $\mathcal{K}$  as

$$\mathcal{K} = \mathcal{W}_0 - \gamma \mathcal{W}_1, \quad (\text{A6})$$

with

$$\mathcal{W}_0 = \begin{bmatrix} \mathbf{W}_0 & \mathbf{0} \\ \mathbf{0} & -\mathbf{W}_0 \end{bmatrix}, \quad (\text{A7})$$

and  $[\mathbf{W}_0]_{\alpha,\beta} = \delta_{\alpha,\beta} \epsilon_\alpha$ , with  $\epsilon_\alpha$  being the corresponding energy eigenvalue of the *disconnected* system, in which one has set  $\gamma = 0$ . A sequence of interconnected equations for the  $\Theta_N$  is generated by singling out the coefficients of the terms at any order in  $\gamma$ , thus obtaining, at the NESS

$$\begin{aligned} D[\Theta_{\text{NESS},0}] &= \mathcal{G} \\ D[\Theta_{\text{NESS},n}] &= -i[\mathcal{W}_1, \Theta_{\text{NESS},n-1}] , \end{aligned} \quad (\text{A8})$$

with  $n \geq 1$ . The solution of Eqs.(A8) can be readily provided in terms of the matrix elements of  $\Theta_{\text{NESS}}$ ,  $[\Theta_{\text{NESS}}]_{\alpha,\beta}$ , with  $\alpha, \beta \in \{(L, k, p), (2K, q, p)\}$  and  $p = \pm 1$  being the Nambu index. As a result, one obtains

$$\begin{aligned} [\Theta_{\text{NESS},0}]_{\alpha,\beta} &= \frac{\mathcal{G}_{\alpha,\beta}}{-i([\mathcal{W}_0]_{\alpha,\alpha} + [\mathcal{W}_0]_{\beta,\beta}) + \frac{1}{2}[\mathcal{G} + \mathcal{R}]_{\alpha,\alpha} + [\mathcal{G} + \mathcal{R}]_{\beta,\beta}} \\ [\Theta_{\text{NESS},n}]_{\alpha,\beta} &= \frac{-i[\mathcal{W}_1, [\Theta_{\text{NESS},n-1}]]_{\alpha,\beta}}{-i([\mathcal{W}_0]_{\alpha,\alpha} + [\mathcal{W}_0]_{\beta,\beta}) + \frac{1}{2}[\mathcal{G} + \mathcal{R}]_{\alpha,\alpha} + [\mathcal{G} + \mathcal{R}]_{\beta,\beta}} . \end{aligned} \quad (\text{A9})$$

On iteratively solving Eqs.(A9) it is possible to compute  $G_{\text{int},n}$ , as we discuss in the following.

## 2. Charge current at the NS interface in the non-equilibrium steady state

We now employ the LME approach to compute  $G_{\text{int},n}$ . To do so, we consider the corresponding current operator, given by

$$J_{\text{int},n} = -i\gamma\{\alpha_{\mathcal{N}}^\dagger \chi_n - \chi_n^\dagger \alpha_{\mathcal{N}}\} . \quad (\text{A10})$$

Using (the inverse of) Eqs.(11,14) of the main text, we may readily express the average interface current at time  $t$ ,  $I_{\text{int},n}(t)$ , in terms of the matrix elements of  $\theta(t)$  and of  $\theta^A(t)$  as

$$\begin{aligned} I_{\text{int},n}(t) &= 2\gamma \Im \text{Tr}[\rho(t) \alpha_{\mathcal{N}}^\dagger \chi_n] \\ &= 2\gamma \sum_{k,q} \sqrt{\frac{2}{\mathcal{N}+1}} \sin(k\mathcal{N}) \\ &\quad \times \Im \{u_{q,n} \theta_{(L,k);(2K,q)}(t) + [v_{q,n}]^* \theta_{(L,k);(2K,q)}^A(t)\} . \end{aligned} \quad (\text{A11})$$

While all the steps we went through so far rely on no specific approximations, in the following we make the assumption that the 2LRK is weakly coupled to the leads, so that we may stop the calculation of the right-hand side of Eq.(A11) to second order in  $\gamma$ . Moreover, since we are interested in the current characterizing the non-equilibrium steady state, we use Eqs.(A9) to compute the corresponding  $\Theta$ -matrix. In order to compute  $I_{\text{int},n}$  to second order in  $\gamma$ , we approximate  $\Theta_{\text{NESS}}$  as  $\Theta_{\text{NESS}} \approx \Theta_{\text{NESS},0} + \gamma \Theta_{\text{NESS},1}$ . From Eq.(A11) we therefore obtain, for the current through site  $n$  in the NESS to order  $\gamma^2$

$$\begin{aligned} I_{\text{int},n} &= 2\gamma^2 \sum_{k,q} \sqrt{\frac{2}{\mathcal{N}+1}} \sin(k\mathcal{N}) \\ &\quad \times \Im \{u_{q,n} [\Theta_{\text{NESS},1}]_{(L,k,1);(2K,q,1)} \\ &\quad + [v_{q,n}]^* [\Theta_{\text{NESS},1}]_{(L,k,-1);(2K,q,1)}\} . \end{aligned} \quad (\text{A12})$$

Integrating over the lead modes, we rewrite the right-hand side of Eq.(A12) as a sum over contributions from the modes of the superconducting chain, that is

$$I_{\text{int},n} = \sum_q I_{\text{int},n}^q , \quad (\text{A13})$$

with

$$\begin{aligned} I_{\text{int},n}^q &= 2\gamma^2 \Gamma \frac{2}{\mathcal{N}+1} \sum_k \left\{ \frac{\sin^2(k\mathcal{N}) |u_{q,n}|^2 (\bar{n}_{L,k} - \bar{n}_{2K,q})}{(\epsilon_{L,k} - \epsilon_{2K,q})^2 + \Gamma^2} \right. \\ &\quad \left. + \frac{\sin^2(k\mathcal{N}) |b_{q,n}|^2 (\bar{n}_{L,k} + \bar{n}_{2K,q} - 1)}{(\epsilon_{L,k} - \epsilon_{2K,q})^2 + \Gamma^2} \right\} , \end{aligned} \quad (\text{A14})$$

with  $\bar{n}_{L,k}$  and  $\bar{n}_{2K,q}$  being respectively the average particle occupancy of the lead level with momentum  $k$  and of the superconductor level with momentum  $q$ . As the result in Eqs.(A12,A13) is independent of the specific Hamiltonian for the Kitaev chain, it keeps valid at any given realization of the disorder in the superconductor. In addition, from Eq.(A14) we find that the leading contribution in  $\gamma$  to  $I_{\text{int},n}$  is given by the sum of two different terms, the former one determined by the subgap, real fermionic modes (if any, that is, if the Kitaev chain is in a topological phase), the latter one, instead, being determined by the “bulk” states, at energy  $\geq \Delta_{2K}$ . In order to have a finite  $I_{\text{int},n}$ , a voltage bias  $V$  has to be applied between the metallic lead and the superconductor. Once we know  $I_{\text{int},n}$  as a function of  $V$ , we define the corresponding dc conductance at site  $n$ ,  $G_{\text{int},n}$ , as  $G_{\text{int},n} = \lim_{V \rightarrow 0} \frac{\partial I_{\text{int},n}}{\partial V}$ .

Just as  $I_{\text{int},n}$ , also  $G_{\text{int},n}$  is typically written as a contribution from the localized edge states plus a contribution from the bulk states. We now prove that, as soon as  $\Delta_{2K}$  is finite, regardless of whether the system is disordered, or not, in the zero-temperature limit the latter contribution is always = 0 in the small- $\gamma$  limit. To evidence this point, we note that, following the same steps as in Ref.[44], we get that the contribution to the total conductance arising from the delocalized (above the gap) states is given by

$$[G_{\text{int},n}]_{\text{bulk}} = \frac{4\gamma^2}{\pi t^2} \sum_q \left[ \frac{|u_{q,n}|^2 |v_{q,n}|^2}{|u_{q,n}|^2 + |v_{q,n}|^2} \right] \left[ \frac{2t\Gamma}{\Gamma^2 + \epsilon_q^2} \right] . \quad (\text{A15})$$

In Eq.(A15) we sum over the full Brillouin zone of the (isolated) Kitaev chain. For a long enough chain, we may trade the sum over  $q$  for an integral over the energies, by introducing the density of state function for the Kitaev chain,  $\rho_{2K}(\epsilon)$ , so that  $\sum_q = \int d\epsilon \rho_{2K}(\epsilon)$ . Let us assume that a generic realization of the disorder potential yields a finite gap  $\Delta_{2K}$  in the spectrum of the superconducting chain. As long as  $\Gamma \ll \Delta_{2K}$ , we may approximate  $\frac{\Gamma}{\Gamma^2 + \epsilon^2} \approx \pi \delta(|\epsilon| - \Gamma)$ . Thus, as there are no

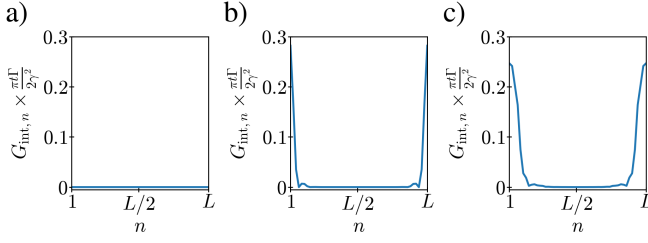


FIG. 9.  $G_{\text{int},n}$  computed in the clean 2LRK, for  $L = 50$  and with  $g = 1$  and, respectively,  $\lambda_1 = \lambda_2 = 0.5$  (panel **a**), corresponding to the topologically trivial phase, with no localized states),  $\lambda_1 = 1.5, \lambda_2 = 0.3$  (panel **b**), corresponding to the topological phase with  $\omega = 1$ ,  $\lambda_1 = 2.0, \lambda_2 = 1.5$  (panel **c**) corresponding to the topological phase with  $\omega = 2$ .

states within the interval  $-\Delta_{2K} \leq \epsilon \leq \Delta_{2K}$ , we readily find that  $[G_{\text{int},n}]_{\text{bulk}} = 0, \forall n$ . Let us, now, consider the contribution to the conductance arising from the subgap boundary states.

As a legitimate eigenstate of the Hamiltonian, each subgap state is described by a Bogoliubov-de Gennes wavefunction in the form  $(u_n, v_n)$ , with  $|u_n| = |v_n|$ . In the large- $L$  limit (long Kitaev chain) we may neglect finite-size corrections to the localized state energies which, accordingly, are stuck at  $\epsilon = 0$ . In this limit and for  $T \rightarrow 0$ , the total contribution to the dc conductance emerging from the localized boundary states is given by

$$[G_{\text{int},n}]_{\text{loc}} = \sum_{\alpha=\text{loc}} \frac{4\gamma^2 |u_{\alpha,n}|^2}{\pi t \Gamma} \left[ 1 + \left( \frac{\Gamma}{2t} \right)^2 \right], \quad (\text{A16})$$

with the sum taken over the set of isolated states.

From our discussion above, we find that, in the dc limit and at low enough temperature, only the subgap modes

(if any) contribute  $G_{\text{int},n}$ . To evidence this result, in Fig.9 we plot the site-dependent conductance computed in the clean Kitaev chain, for  $L = 50$  and with  $g = 1$  and, respectively,  $\lambda_1 = \lambda_2 = 0.5$  (panel **a**), corresponding to the topologically trivial phase, with no localized states),  $\lambda_1 = 1.5, \lambda_2 = 0.3$  (panel **b**), corresponding to the topological phase with a single subgap real fermionic mode at each endpoint of the chain),  $\lambda_1 = 2.0, \lambda_2 = 1.5$  (panel **c**) corresponding to two subgap real fermionic modes localized at each endpoint of the chain). From the three plots, we readily note that  $G_{\text{int},n}$  is practically 0 in the trivial phase and in the bulk of the topological phases. At variance, close to the boundaries of the chain, it jumps to a finite value ( $\propto \frac{\gamma^2}{\pi t \Gamma}$ ), following the profile of  $|u_{\alpha,n}|^2$  for the localized boundary states (note that for every subgap localized state we have  $|u_{\alpha,n}|^2 = |v_{\alpha,n}|^2$ ). Summing over  $n$ , the normalization condition for the localized state wavefunctions yields

$$G_{\text{int}} = \sum_{n=1}^L G_{\text{int},n} = \frac{2\gamma^2}{\pi t \Gamma} \left[ 1 + \left( \frac{\Gamma}{2t} \right)^2 \right] \omega, \quad (\text{A17})$$

with  $\omega$  counting the number of subgap, real fermionic modes localized at each boundary of the chain. Thus, we conclude that a zero/finite value of  $G_{\text{int}}$  evidences the absence/presence of the subgap modes characterizing the topological phases of the Kitaev chain, marking the phase transition lines with abrupt (and quantized) jumps in its value. As we discuss in the main text, on such an observation we ground our method to map out the phase diagram of the disordered 2LRK by looking at the (disorder averaged) dc conductance as a function of the system parameters.

- 
- [1] M. Z. Hasan and C. L. Kane, Colloquium: Topological insulators, *Rev. Mod. Phys.* **82**, 3045 (2010).
  - [2] X.-L. Qi and S.-C. Zhang, Topological insulators and superconductors, *Rev. Mod. Phys.* **83**, 1057 (2011).
  - [3] G. Moore and N. Read, Nonabelions in the fractional quantum hall effect, *Nuclear Physics B* **360**, 362 (1991).
  - [4] C. Nayak, S. H. Simon, A. Stern, M. Freedman, and S. Das Sarma, Non-abelian anyons and topological quantum computation, *Rev. Mod. Phys.* **80**, 1083 (2008).
  - [5] Y. Oreg, G. Refael, and F. von Oppen, Helical liquids and majorana bound states in quantum wires, *Phys. Rev. Lett.* **105**, 177002 (2010).
  - [6] Topologically protected elastic waves in phononic metamaterials, *Nature Communications* **6**, 8682 (2015).
  - [7] B. G.-g. Chen, B. Liu, A. A. Evans, J. Paulose, I. Cohen, V. Vitelli, and C. D. Santangelo, Topological mechanics of origami and kirigami, *Phys. Rev. Lett.* **116**, 135501 (2016).
  - [8] F. Cardano, A. D'Errico, A. Dauphin, M. Maffei, B. Piccirillo, C. de Lisio, G. De Filippis, V. Cataudella, E. Santamato, L. Marrucci, M. Lewenstein, and P. Massignan, Detection of zak phases and topological invariants in a chiral quantum walk of twisted photons, *Nature Communications* **8**, 15516 (2017).
  - [9] A. D'Errico, F. Di Colandrea, R. Barboza, A. Dauphin, M. Lewenstein, P. Massignan, L. Marrucci, and F. Cardano, Bulk detection of time-dependent topological transitions in quenched chiral models, *Phys. Rev. Res.* **2**, 023119 (2020).
  - [10] J. Zak, Berry's phase for energy bands in solids, *Phys. Rev. Lett.* **62**, 2747 (1989).
  - [11] L. Fidkowski, T. S. Jackson, and I. Klich, Model characterization of gapless edge modes of topological insulators using intermediate brillouin-zone functions, *Phys. Rev. Lett.* **107**, 036601 (2011).
  - [12] B.-H. Chen and D.-W. Chiou, An elementary rigorous proof of bulk-boundary correspondence in the generalized su-schrieffer-heeger model, *Physics Letters A* **384**, 126168 (2020).
  - [13] L. Li, Z. Xu, and S. Chen, Topological phases of generalized su-schrieffer-heeger models, *Phys. Rev. B* **89**, 085111 (2014).



- [14] C. Li and A. E. Miroshnichenko, Extended ssh model: Non-local couplings and non-monotonous edge states, *Physics* **1**, 2 (2019).
- [15] R. K. Malakar and A. K. Ghosh, Engineering topological phases of any winding and chern numbers in extended su-schrieffer-heeger models, *Journal of Physics: Condensed Matter* **35**, 335401 (2023).
- [16] B. Pérez-González, M. Bello, A. Gómez-León, and G. Platero, Interplay between long-range hopping and disorder in topological systems, *Phys. Rev. B* **99**, 035146 (2019).
- [17] Y. Niu, S. B. Chung, C.-H. Hsu, I. Mandal, S. Raghu, and S. Chakravarty, Majorana zero modes in a quantum ising chain with longer-ranged interactions, *Phys. Rev. B* **85**, 035110 (2012).
- [18] W. DeGottardi, M. Thakurathi, S. Vishveshwara, and D. Sen, Majorana fermions in superconducting wires: Effects of long-range hopping, broken time-reversal symmetry, and potential landscapes, *Phys. Rev. B* **88**, 165111 (2013).
- [19] S. Lieu, D. K. K. Lee, and J. Knolle, Disorder protected and induced local zero-modes in longer-range kitaev chains, *Phys. Rev. B* **98**, 134507 (2018).
- [20] X.-S. Li, J.-R. Li, S.-F. Zhang, L.-L. Zhang, and W.-J. Gong, Topological properties of the dimerized kitaev chain with long-range couplings, *Results in Physics* **30**, 104837 (2021).
- [21] Z.-W. Zuo and D. Kang, Reentrant localization transition in the su-schrieffer-heeger model with random-dimer disorder, *Phys. Rev. A* **106**, 013305 (2022).
- [22] J. Li, R.-L. Chu, J. K. Jain, and S.-Q. Shen, Topological anderson insulator, *Phys. Rev. Lett.* **102**, 136806 (2009).
- [23] E. G. Cinnirella, A. Nava, G. Campagnano, and D. Giuliano, Fate of high winding number topological phases in the disordered extended su-schrieffer-heeger model, *Phys. Rev. B* **109**, 035114 (2024).
- [24] F. Pientka, A. Romito, M. Duckheim, Y. Oreg, and F. v. Oppen, Signatures of topological phase transitions in mesoscopic superconducting rings, *New Journal of Physics* **15**, 025001 (2013).
- [25] A. Nava, R. Giuliano, G. Campagnano, and D. Giuliano, Persistent current and zero-energy majorana modes in a  $p$ -wave disordered superconducting ring, *Phys. Rev. B* **95**, 155449 (2017).
- [26] E. G. Cinnirella, A. Nava, G. Campagnano, and D. Giuliano, Phase diagram of the disordered kitaev chain with long-range pairing connected to external baths, *Phys. Rev. B* **111**, 155149 (2025).
- [27] S.-N. Liu, G.-Q. Zhang, L.-Z. Tang, and D.-W. Zhang, Topological anderson insulators induced by random binary disorders, *Physics Letters A* **431**, 128004 (2022).
- [28] A. Nava, G. Campagnano, P. Sodano, and D. Giuliano, Lindblad master equation approach to the topological phase transition in the disordered su-schrieffer-heeger model, *Phys. Rev. B* **107**, 035113 (2023).
- [29] P. G. Harper, Single band motion of conduction electrons in a uniform magnetic field, *Proceedings of the Physical Society. Section A* **68**, 874 (1955).
- [30] S. Aubry and G. André, Analyticity breaking and anderson localization in incommensurate lattices, *Ann. Israel Phys. Soc* **3**, 18 (1980).
- [31] G. Lindblad, On the generators of quantum dynamical semigroups, *Communications in Mathematical Physics* **48**, 119 (1976).
- [32] S. Diehl, E. Rico, M. A. Baranov, and P. Zoller, Topology by dissipation in atomic quantum wires, *Nature Physics* **7**, 971 (2011).
- [33] M. Goldstein, Dissipation-induced topological insulators: A no-go theorem and a recipe, *SciPost Phys.* **7**, 067 (2019).
- [34] G. Shavit and M. Goldstein, Topology by dissipation: Transport properties, *Phys. Rev. B* **101**, 125412 (2020).
- [35] T. Cui, X. Yang, C. Vaswani, J. Wang, R. M. Fernandes, and P. P. Orth, Impact of damping on the superconducting gap dynamics induced by intense terahertz pulses, *Phys. Rev. B* **100**, 054504 (2019).
- [36] A. Nava, C. A. Perroni, R. Egger, L. Lepori, and D. Giuliano, Lindblad master equation approach to the dissipative quench dynamics of planar superconductors, *Phys. Rev. B* **108**, 245129 (2023).
- [37] A. Nava, C. A. Perroni, R. Egger, L. Lepori, and D. Giuliano, Dissipation-driven dynamical topological phase transitions in two-dimensional superconductors, *Phys. Rev. B* **109**, L041107 (2024).
- [38] M. de Leeuw, C. Paletta, B. Pozsgay, and E. Vernier, Hidden quasilocal charges and gibbs ensemble in a lindblad system, *Phys. Rev. B* **109**, 054311 (2024).
- [39] F. Tarantelli and E. Vicari, Quantum critical systems with dissipative boundaries, *Phys. Rev. B* **104**, 075140 (2021).
- [40] I. Pizorn, One-dimensional bose-hubbard model far from equilibrium, *Phys. Rev. A* **88**, 043635 (2013).
- [41] G. Benenti, G. Casati, T. Prosen, and D. Rossini, Negative differential conductivity in far-from-equilibrium quantum spin chains, *Europhysics Letters* **85**, 37001 (2009).
- [42] G. Benenti, G. Casati, T. c. v. Prosen, D. Rossini, and M. Žnidarič, Charge and spin transport in strongly correlated one-dimensional quantum systems driven far from equilibrium, *Phys. Rev. B* **80**, 035110 (2009).
- [43] A. Nava, M. Rossi, and D. Giuliano, Lindblad equation approach to the determination of the optimal working point in nonequilibrium stationary states of an interacting electronic one-dimensional system: Application to the spinless hubbard chain in the clean and in the weakly disordered limit, *Phys. Rev. B* **103**, 115139 (2021).
- [44] P. H. Guimarães, G. T. Landi, and M. J. de Oliveira, Nonequilibrium quantum chains under multisite lindblad baths, *Phys. Rev. E* **94**, 032139 (2016).
- [45] A. Maiellaro, F. Romeo, C. A. Perroni, V. Cataudella, and R. Citro, Unveiling signatures of topological phases in open kitaev chains and ladders, *Nanomaterials* **9**, 10.3390/nano9060894 (2019).
- [46] A. Y. Kitaev, Unpaired majorana fermions in quantum wires, *Physics-Uspekhi* **44**, 131 (2001).
- [47] R. M. Lutchyn, J. D. Sau, and S. Das Sarma, Majorana fermions and a topological phase transition in semiconductor-superconductor heterostructures, *Phys. Rev. Lett.* **105**, 077001 (2010).
- [48] J. D. Sau and S. D. Sarma, Realizing a robust practical majorana chain in a quantum-dot-superconductor linear array, *Nature Communications* **3**, 964 (2012).
- [49] T. Dvir, G. Wang, N. van Loo, C.-X. Liu, G. P. Mazur, A. Bordin, S. L. D. ten Haaf, J.-Y. Wang, D. van Driel, F. Zatelli, X. Li, F. K. Malinowski, S. Gazibegovic, G. Badawy, E. P. A. M. Bakkers, M. Wimmer, and L. P. Kouwenhoven, Realization of a minimal kitaev chain in coupled quantum dots, *Nature* **614**, 445 (2023).

- [50] K. Chhajed, From ising model to kitaev chain, [Resonance](#) **26**, 1539 (2021).
- [51] D. Vodola, L. Lepori, E. Ercolessi, A. V. Gorshkov, and G. Pupillo, Kitaev chains with long-range pairing, [Phys. Rev. Lett.](#) **113**, 156402 (2014).
- [52] O. Viyuela, D. Vodola, G. Pupillo, and M. A. Martin-Delgado, Topological massive dirac edge modes and long-range superconducting hamiltonians, [Phys. Rev. B](#) **94**, 125121 (2016).
- [53] L. Lepori, D. Vodola, G. Pupillo, G. Gori, and A. Trombettoni, Effective theory and breakdown of conformal symmetry in a long-range quantum chain, [Annals of Physics](#) **374**, 35 (2016).
- [54] D. Giuliano, S. Paganelli, and L. Lepori, Current transport properties and phase diagram of a kitaev chain with long-range pairing, [Phys. Rev. B](#) **97**, 155113 (2018).
- [55] F. Pientka, L. I. Glazman, and F. von Oppen, Topological superconducting phase in helical shiba chains, [Phys. Rev. B](#) **88**, 155420 (2013).
- [56] F. Pientka, L. I. Glazman, and F. von Oppen, Unconventional topological phase transitions in helical shiba chains, [Phys. Rev. B](#) **89**, 180505 (2014).
- [57] D. Giuliano, P. Sodano, A. Tagliacozzo, and A. Trombettoni, From four- to two-channel kondo effect in junctions of xy spin chains, [Nuclear Physics B](#) **909**, 135 (2016).
- [58] P. W. Brouwer, M. Duckheim, A. Romito, and F. von Oppen, Probability distribution of majorana end-state energies in disordered wires, [Phys. Rev. Lett.](#) **107**, 196804 (2011).
- [59] F. Pientka, G. Kells, A. Romito, P. W. Brouwer, and F. von Oppen, Enhanced zero-bias majorana peak in the differential tunneling conductance of disordered multi-subband quantum-wire/superconductor junctions, [Phys. Rev. Lett.](#) **109**, 227006 (2012).
- [60] I. Mondragon-Shem, T. L. Hughes, J. Song, and E. Prodan, Topological criticality in the chiral-symmetric aiii class at strong disorder, [Phys. Rev. Lett.](#) **113**, 046802 (2014).
- [61] A. Tadjine and C. Delerue, Anderson localization induced by gauge-invariant bond-sign disorder in square pbse nanocrystal lattices, [Phys. Rev. B](#) **98**, 125412 (2018).
- [62] F. Schwarz, M. Goldstein, A. Dorda, E. Arrigoni, A. Weichselbaum, and J. von Delft, Lindblad-driven discretized leads for nonequilibrium steady-state transport in quantum impurity models: Recovering the continuum limit, [Phys. Rev. B](#) **94**, 155142 (2016).
- [63] M. Lotem, A. Weichselbaum, J. von Delft, and M. Goldstein, Renormalized lindblad driving: A numerically exact nonequilibrium quantum impurity solver, [Phys. Rev. Res.](#) **2**, 043052 (2020).
- [64] N. Leumer, M. Grifoni, B. Muralidharan, and M. Marganska, Linear and nonlinear transport across a finite kitaev chain: An exact analytical study, [Phys. Rev. B](#) **103**, 165432 (2021).
- [65] A. D’Abbruzzo and D. Rossini, Topological signatures in a weakly dissipative kitaev chain of finite length, [Phys. Rev. B](#) **104**, 115139 (2021).
- [66] O. Motrunich, K. Damle, and D. A. Huse, Griffiths effects and quantum critical points in dirty superconductors without spin-rotation invariance: One-dimensional examples, [Phys. Rev. B](#) **63**, 224204 (2001).
- [67] S.-k. Ma, C. Dasgupta, and C.-k. Hu, Random antiferromagnetic chain, [Phys. Rev. Lett.](#) **43**, 1434 (1979).
- [68] C. Dasgupta and S.-k. Ma, Low-temperature properties of the random heisenberg antiferromagnetic chain, [Phys. Rev. B](#) **22**, 1305 (1980).
- [69] D. S. Fisher, Random transverse field ising spin chains, [Phys. Rev. Lett.](#) **69**, 534 (1992).
- [70] G. A. Domínguez-Castro and R. Paredes, The aubry-andré model as a hobbyhorse for understanding the localization phenomenon, [European Journal of Physics](#) **40**, 045403 (2019).
- [71] V. Berger, A. Nava, J. H. Bardarson, and C. Artiago, Numerical study of disordered noninteracting chains coupled to a local lindblad bath (2024), [arXiv:2412.03233 \[cond-mat.dis-nn\]](#).
- [72] J. Fraxanet, U. Bhattacharya, T. Grass, D. Rakshit, M. Lewenstein, and A. Dauphin, Topological properties of the long-range kitaev chain with aubry-andré-harper modulation, [Phys. Rev. Res.](#) **3**, 013148 (2021).
- [73] R. Nehra, A. Sharma, and A. Soori, Transport in a long-range kitaev ladder: Role of majorana and subgap andreev states, [Europhysics Letters](#) **130**, 27003 (2020).
- [74] D. Guerzi and A. Nava, Probing majorana zero modes by measuring transport through an interacting magnetic impurity, [Physica E: Low-dimensional Systems and Nanostructures](#) **134**, 114895 (2021).
- [75] A. Langari, A. Mohammad-Aghaei, and R. Haghsheenas, Quantum phase transition as an interplay of kitaev and ising interactions, [Phys. Rev. B](#) **91**, 024415 (2015).
- [76] B.-Z. Zhou and B. Zhou, Topological phase transition in a ladder of the dimerized kitaev superconductor chains, [Chinese Physics B](#) **25**, 107401 (2016).